Journal of Rock Mechanics and Geotechnical Engineering 7 (2015) 519–531

Contents lists available at ScienceDirect

Journal of Rock Mechanics and Geotechnical Engineering

journal homepage: www.rockgeotech.org

Full length article

A borehole stability study by newly designed laboratory tests on thick-walled hollow cylinders

S.S. Hashemi*, N. Melkoumian, A. Taheri

Deep Exploration Technologies Cooperative Research Centre, School of Civil, Environmental and Mining Engineering, University of Adelaide, Adelaide, Australia

ARTICLE INFO

Article history:
Received 25 March 2015
Received in revised form
4 June 2015
Accepted 9 June 2015
Available online 30 July 2015

Keywords:
Real-time monitoring
Experimental investigation
Thick-walled hollow cylinder (TWHC)
Poorly cemented sand formations

ABSTRACT

At several mineral exploration drilling sites in Australia, weakly consolidated formations mainly consist of sand particles that are poorly bonded by cementing agents such as clay, iron oxide cement or calcite. These formations are being encountered when drilling boreholes to the depth of up to 200 m. To study the behaviour of these materials, thick-walled hollow cylinder (TWHC) and solid cylindrical synthetic specimens were designed and prepared by adding Portland cement and water to sand grains. The effects of different parameters such as water and cement contents, grain size distribution and mixture curing time on the characteristics of the samples were studied to identify the mixture closely resembling the formation at the drilling site. The Hoek triaxial cell was modified to allow the visual monitoring of grain debonding and borehole breakout processes during the laboratory tests. The results showed the significance of real-time visual monitoring in determining the initiation of the borehole breakout. The size-scale effect study on TWHC specimens revealed that with the increasing borehole size, the ductility of the specimen decreases, however, the axial and lateral stiffnesses of the TWHC specimen remain unchanged. Under different confining pressures the lateral strain at the initiation point of borehole breakout is considerably lower in a larger size borehole (20 mm) compared to that in a smaller one (10 mm). Also, it was observed that the level of peak strength increment in TWHC specimens decreases with the increasing confining pressure.

1. Introduction

Borehole stability analysis is an important issue for researchers in the field of geotechnical, mining and petroleum engineering. Several borehole instability problems during or after the completion of drilling have been reported by a number of exploration companies in Australia. Many of these problems were reported in drilling projects in poorly cemented sand formations at the depth of up to 200 m beneath the ground. The sand production problem, as it is known, has also been observed in weakly bonded sandstones where the debonding of sand grains can be triggered by fluid pressure and induced stresses leading to the failure of sandstone at the borehole wall (Geertsma, 1985; Perkins and Weingarten, 1988). The strength of a granular material formation is generated mainly by a natural cementing agent that bonds sand grains together (Al-Awad et al., 1999).

In recent decades, a number of numerical and experimental studies have been conducted on borehole stability in different rock formations. Gough and Bell (1982) showed that, in a large number of vertical oil wells, the orientation of consistent breakouts coincides with the direction of the regional minimum horizontal principal stress. Numerical studies on poorly cemented sand formation by Hashemi et al. (2014a, b) revealed that breakage of weak bonding between sand particles causes instability and sand grains remain intact in the case of a borehole failure. In laboratory conditions it was shown that borehole breakouts grow mainly through radial penetration into the rock mass without any circumferential extension (Lee and Haimson, 1993). Haimson and Song (1993) conducted laboratory tests on two varieties of Berea sandstones with 17% and 22% porosity, respectively, and revealed two distinct breakout patterns directly related to the microstructures of these rocks and their different modes of failure. Microscopic observation by Hagin and Zoback (2004) revealed that the fundamental mechanism behind sand production is the growth of small, opening-mode and splitting cracks oriented parallel to the tangential stress, starting very close to the borehole wall and propagating deeper into the matrix with increasing stress. Similar

* Corresponding author. Tel.: +61 426111280; fax: +61 883134359.
E-mail address: shashemi@civeng.adelaide.edu.au (S.S. Hashemi).

Peer review under responsibility of Institute of Rock and Soil Mechanics, Chinese Academy of Sciences.
1674-7755
http://dx.doi.org/10.1016/j.jrmge.2015.06.005

borehole instabilities have also been documented by many other authors (Fischer et al., 1978; Ewy and Cook, 1990a, b; Chang et al., 1997; Al-Ajmi and Zimmerman, 2006).

Unconfined compressive strength triaxial and thick-walled hollow cylinder (TWHC) tests are two of the most useful laboratory experiments (King, 1912; Robertson, 1955; Hoskins, 1969; Adeyanju and Olafuyi, 2011). The geometry of the TWHC allows the application of various load path combinations to simulate stress conditions around boreholes. The classical hollow cylinder approach is not well suited to investigating the stability of poorly cemented formations because, during or subsequent to these tests, the instability of the weak sandstone arch and the grain debonding process in sandy formations cannot be captured. The hollow cylinder tests on an intact rock sample focus mainly on rupture phenomena such as shear and tensile failure (Hall and Harrisberger, 1970; Tippieand and Kohlhaas, 1973; Cleary et al., 1979).

In this study, a series of newly designed laboratory tests involving real-time monitoring of the development of breakout in an unsupported borehole was conducted. The paper aims to provide a more accurate representation of the actual behaviour of poorly cemented sands, which will be invaluable in designing appropriate borehole support systems. The tests were conducted on specimens of poorly cemented sands prepared in laboratory and the effects of different mixture characteristics (i.e. proportion of sand, cement and water) on their mechanical behaviours were studied by conducting compression tests on solid and hollow cylindrical specimens.

2. Drilling field investigation

Exploration boreholes are usually drilled to uncover potential future mine sites. In many cases, drilling is undertaken through poorly cemented sand formations. Generally, the boreholes are 250–300 mm in diameter and 50–200 m in length, depending on the underground conditions in Australia. This study focuses on solid and TWHC laboratory test specimens based on disturbed samples collected from a problematic drilling site at Burra, South Australia. At this site the sediment above bedrock is heterogeneous, with the shallower layers composed of silt and fine sand and the deeper layers transition to dark grey plastic clay. The problematic, poorly cemented sandstone underlies this clayey layer and consists of sand particles with a weak cementation due to the presence of iron dioxide, clay and calcite (Fig. 1). Quartz grains are mostly fine and sub-angular with random orientations. The yellowish-grey specimens were prepared in laboratory so that their fabric closely resembles that of the poorly cemented sands at the drilling site.

To drill a borehole at this site, different drilling methods have been tried to minimise the risk of borehole failure. In some cases, drilling mud has been used to maintain an open borehole during drilling. However, to conduct further investigation, some boreholes need to remain open for several months after drilling. The air core drilling and reverse circulation drilling methods were used in these cases. These are dry drilling methods and have been conventionally applied to drilling through soft ground in Australia. The cuttings are conveyed to the surface and pass through the sample collection system from where they are collected. Drilling continues with the addition of rods to the top of the drill string. When the drilling string reaches the poorly cemented sand layer, the borehole may collapse if the bonding between sand particles is not strong enough to provide stability. According to the reports from drilling company, the main factors affecting borehole instability include the low strength of poorly cemented sands which cannot sustain the existing in-situ stress after drilling, and, in few cases, fluid flow due to a confined aquifer near the borehole collapse zone.

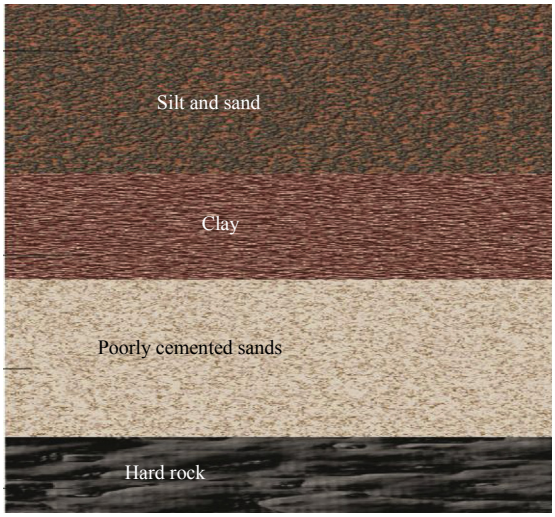

Fig. 1. Vertical geological cross-section near Burra, South Australia (Hashemi et al., 2014a, b).

3. Thick-walled hollow cylinders (TWHCs)

Hollow cylinder specimens were first used in the early 20th century when the importance of adopting a realistic model was identified for an underground opening. The opening was located at a depth of 9.5 km and susceptible to collapse due to high in-situ stresses (Hoskins, 1969). Since then, a wide range of experimental investigations involving hollow cylindrical specimens has been conducted. Robertson (1955) studied the effect of the inner-to-outer diameter ratio on the strength of various rocks. King (1912) analysed the system of fractures that might develop during compressive tests on hollow cylinder specimens under different stress states. Bridgman (1952) performed hollow cylinder tests under different loadings. Pomeroy and Hobbs (1962) examined the strength of hollow cylinder coal specimens. Mazanti and Sowers (1966) studied the behaviour of hollow cylinder granite specimens and the effect of the intermediate principal stress (σ_2) on their strength. Ewy et al. (1988) studied the deformation and fracture development in a hard rock around a borehole using TWHC tests. These and other work involving TWHC tests show that the TWHC configuration tests are well suited for identifying and investigating both the macro- and micro-properties of different rock types.

Depending on the thickness of a hollow cylinder specimen, stresses that develop in its wall due to the application of uniform stresses can be analysed by two different methods. In a TWHC specimen, the wall thickness, t, which is much smaller in comparison to its inner diameter, D_i (i.e. $D_i > 20t$), the stresses that distribute across the specimen walls can be considered almost homogeneous and uniform. This assumption is not fully acceptable in the case of a thick-walled hollow specimen, the wall thickness of which is larger in comparison to its inner diameter. In the latter case, stress distribution is not homogenous in the specimen wall. In many textbooks (e.g. Obert and Duvall, 1967; Jaeger et al., 2007) closed form solutions based on the linear theory of elasticity for calculating stresses and strains in both thin- and thick-walled hollow cylinder specimens were presented. For a TWHC with an inner diameter of D_i, outer diameter of D_o and length of L, subjected to axial force (F), uniform internal stress s_i and external stress s_o, the principal stresses at any point at a radial distance r from the centre of the specimen can be presented in cylindrical coordinates as follows (Jaeger et al., 2007):

$$\sigma_{\theta\theta} = \frac{s_o D_o^2 - s_i D_i^2}{D_o^2 - D_i^2} + \frac{(s_o - s_i) D_i^2 D_o^2}{4r^2\left(D_o^2 - D_i^2\right)} \quad (1)$$

$$\sigma_{rr} = \frac{s_o D_o^2 - s_i D_i^2}{D_o^2 - D_i^2} - \frac{(s_o - s_i) D_i^2 D_o^2}{4r^2\left(D_o^2 - D_i^2\right)} \quad (2)$$

$$\sigma_z = \frac{4F}{\pi\left(D_o^2 - D_i^2\right)} + \frac{s_i D_i^2}{D_o^2 - D_i^2} \quad (3)$$

where $\sigma_{\theta\theta}$, σ_{rr} and σ_z are the tangential, radial and axial principal stresses, respectively, which are assumed to be uniformly distributed over the specimen on top and bottom end surfaces (Fig. 2).

4. Experimental study

Laboratory test facilities that were used in the current experimental testing comprised the following components:

(1) Specimens that were both of a reasonable diameter and of a borehole wall thickness satisfying the TWHC theory condition (i.e. $D_i < 20t$) were used. Hence, a HQ Hoek triaxial cell of 63.5 mm in diameter and 127 mm in height was utilised.
(2) A servo-controlled axial loading system of 100 kN loading capacity with 0.1 N accuracy was used for applying vertical stress to the specimen.
(3) Although the Hoek cell was originally designed to apply high confining pressures to hard rock specimens, the hydraulic pressure gauge was modified to allow measuring the confining pressure at very low amounts. An automatic hydraulic machine was used in conjunction with a relief valve and a pressure gauge for applying and maintaining the external confining pressure. Since the maximum confining pressure adopted in the current tests was low (6 MPa), a pressure gauge with an accuracy of 0.01 MPa was used.

The TWHC specimens, consisting of poorly cemented sands, cannot be retrieved from the cell after the destructive tests due to the development of a large number of macro- and micro-cracks and the debonding of sand particles. In addition, the specimen is attached to the membrane and completely crumbles when moved. Thus, it is not possible to retrieve poorly cemented sand specimens and investigate the failure mechanism of borehole after the test. To address this issue, the triaxial cell was modified to allow simultaneous capturing of the borehole failure mechanism and the process of sand grain debonding at each time step and at different stress paths. A micro-camera with a 225 pixel per inch (ppi) resolution was installed inside the hollow platen to record the process of sand debonding and borehole breakout. The micro-camera was connected to a personal computer to record the borehole conditions throughout the test. A 60-channel data acquisition system was connected to two additional personal computers for recording and storing data.

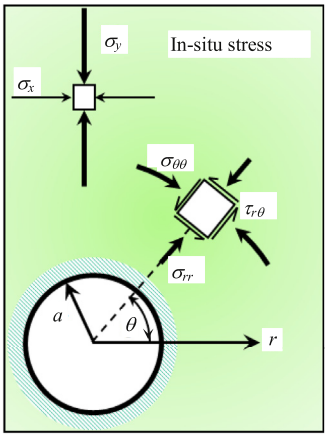

Fig. 2. In-situ stresses on an element at a radial distance r from a drilled borehole centre in polar coordinates.

Initially, three PVC moulds with a slot on the circumference were manufactured to prepare the specimens. However, during the compaction process, the body of the mould bulged and this deformation prevented the specimens from obtaining a uniform cylindrical shape. An additional problem was observed during de-moulding. Since the specimens were very weak, deformation of the mould to release the specimen imparted damage to it. To address this issue, steel moulds were designed and manufactured (Fig. 3a). The dimensions of the moulds were 127 mm in length and 62.5 mm in diameter. Two removable steel dowels with the diameters of 25 mm and 10 mm were used together with the moulds. These dowels were embedded in the mould to create the borehole in the specimens. As shown in Fig. 3a, to avoid damaging the specimen during de-moulding, the moulds comprised two half-cylinders that were joined together by two screws. In addition, the dowels were wrapped in a plastic film (Mayla plastic) and the inner surface of moulds was lubricated with grease (containing a petroleum jelly mixture and stearic acid) which would not penetrate into the mixture. The bottom platens of the moulds were coated with an anti-rust paint to diminish the effect of lubrication. It was observed that unlike the concrete, the strength of the poorly cemented sand specimens was strongly influenced by the mould conditions.

Kongsukprasert (2003) showed that the strength of poorly cemented sand samples is a function of the density of the mixture. Since there was insufficient space between the mould's inner wall and the internal dowel to facilitate compaction, a tool was designed and manufactured to uniformly compact the mixture, as shown in Fig. 3b. Each specimen was compacted in three separate layers of equal thickness (42 mm). The compaction energy for each impact was maintained constant and equal to 0.35 N m/cm^3, which was calculated based on the applied force of the manufactured compactor. Before placing the next layer, the surface of the previously compacted layer was scarified to increase the interlocking between successive layers. To minimise the bedding error effect for the very top layer, a collar was used allowing this layer to achieve conditions similar to those of the lower layers (see Fig. 3a). To avoid the initial setting of the cement for all specimens, the compaction time was strictly maintained at 20–30 min. The compaction began when water was first added to the mixture and was completed when the final layer was compacted.

Two sets of cylindrical platens were manufactured from hardened steel and were hardened prior to crushing and lapping. The platens were designed using the finite element analysis software ABAQUS 6.11 and loading steps similar to those applied during test conditions were applied to the model (Fig. 4). According to the results of simulated platens, the strain of the platens was less than 0.01% with the application of the maximum load of 100 kN. This is far greater than the predicted strength of the specimens. Each platen was designed with a tapered hole, 35 mm at the top and 25 mm or 10 mm at the bottom based on the TWHC specimen hole size. In addition, a small base was fitted to the platen to fix the camera in the position at a small distance above the specimen. The bottom platens were fitted with a uniform cylindrical hole of

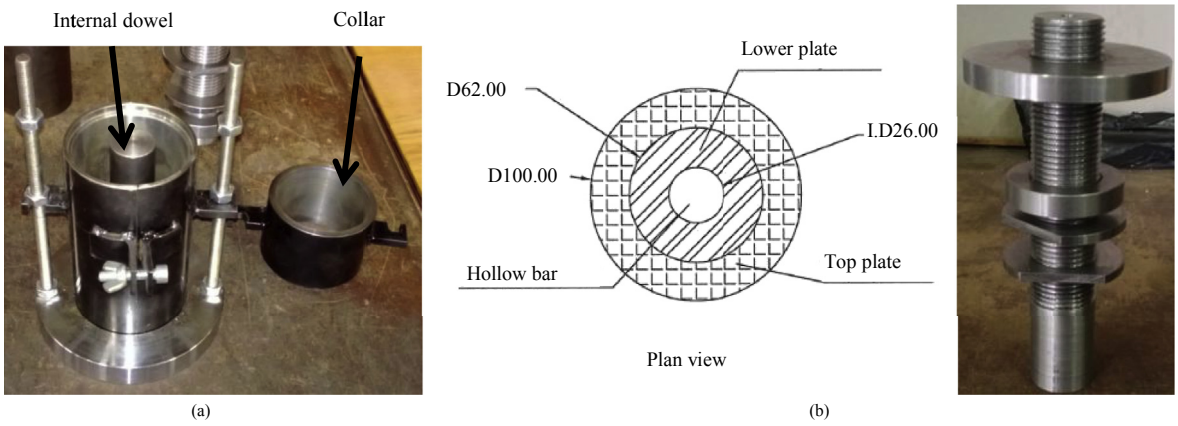

Fig. 3. Apparatus developed to prepare the specimens: (a) Special moulds for preparing TWHC specimens; and (b) Special device for compacting the mixture in the mould uniformly (sizes in mm).

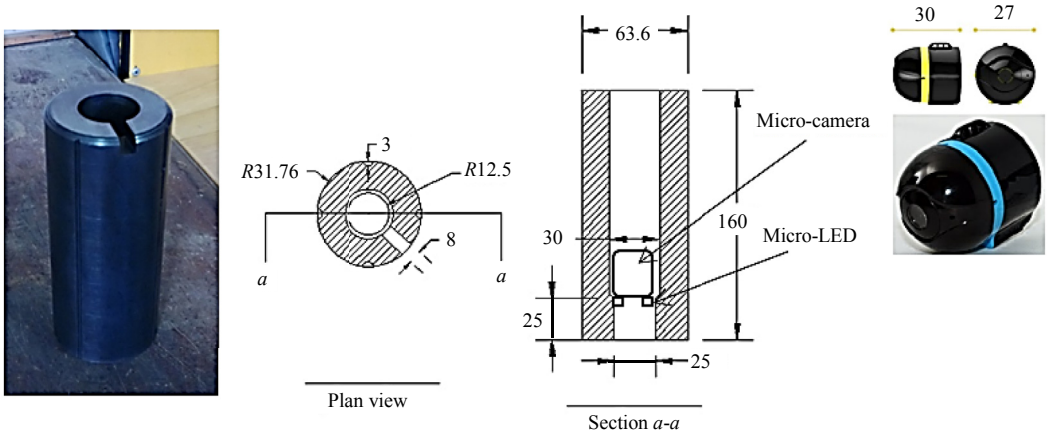

Fig. 4. The designed and manufactured top and bottom platens (unit: mm).

20 mm or 10 mm in diameter, which can be fitted to the bottom ram of the loading machine. These platens were also simulated in ABAQUS. Sand particles, which were debonded from the borehole walls during the test, were allowed to fall onto the bottom platen.

Since the specimens were weak enough to simulate the poorly cemented sand at the drilling site, they were vulnerable to disturbance prior to loading. To avoid applying the weight of the triaxial cell to the specimen during the test, a wooden base was manufactured to support the weight of the triaxial cell. Thus, there was no need to apply an external pressure on the specimens to hold the triaxial set before transferring it to the loading machine.

4.1. Test procedure and setup

The cell was placed on the wooden base and the bottom hollow platen mounted by the loading machine manually ensured that it can move freely inside the Hoek cell. A thin black membrane was used at the end of the bottom hollow platen to ensure that the LED lights of the camera are not reflected during video recording. Both ends of the specimen were then levelled by applying a thin layer of dental paste and, after it had been set, lubricated with a special grease to reduce the friction between the platen and the specimen, thus limiting stress concentration and bedding error. During the setting of the dental paste, the specimen was wrapped in a plastic film to avoid excessive drying of its surface, which could result in the loosening of particles. After the dental paste had been set, precise measurements of the specimen's weight, height and diameter were taken at three different points by means of a calliper.

Measuring the dental paste deformations at the top and bottom surfaces of the specimen during the test revealed that the dental paste could withstand, without any noticeable deformation, a force of up to 100 kN, which is far greater than the strength of the poorly cemented specimen. The results from the preliminary tests on the specimens without capping were not reproducible due to the significant inconsistency in the results.

The top hollow platen was positioned on the specimen and two spherical platens were placed on top of it to ensure that the vertical stress was uniformly applied to the specimen. Pairs of axial and lateral strain gauges were used to measure local deformations on the specimen. Two linear-variable differential transformers (LVDTs) were installed between the top and bottom rams of the loading machine to measure axial displacement externally. Prior to the test, the upper machine ram was brought to the edge of the top platen to set the offsets and 5 N was applied to ensure the contact between the top ram and the hollow platen. The captured image of the micro-camera was checked to ensure that the focal length of the lens was on the middle of the specimen hole and the position of the LEDs was controlled to ensure the borehole illumination was suitable for recording. In the first stage of loading, the vertical and confining stresses were increased simultaneously up to a certain stress level, which simulates the hydrostatic condition on the specimen boundary. Then, in the second stage, the sample was subjected to vertical compression at a constant displacement rate

of 0.07 mm/min. The effects of various strain rates (0.02–0.1 mm/min) were also examined. No significant change was observed in the strength and strain behaviours of the specimens within this strain range. Data were recorded at 0.5 s time intervals.

As has been reported by various drilling companies, time is a key factor in predicting the borehole stability after drilling or when withdrawing the drilling rods from the borehole to change the drilling bit. The video capture software was synchronised with the data acquisition system to facilitate the observation of the sand particle debonding process in parallel with the stress and strain measurements.

Several sets of synthetic mixtures of poorly cemented sands were prepared and tested with different cement-to-sand ratios (by weight), w_c, coarse-to-fine sand particle ratios, δ, and grain size ranges.

4.2. Grain size distribution

To determine typical grain size distributions, samples were collected from the depth of up to 100 m at the drilling site in Burra, South Australia, and sieve analyses were performed using ASTM C-136 calibrated sieves plus pan. The particle size distribution was found to be almost uniform fine grained. Based on these sieve analysis results, natural silica sands (99.6% of silica) of two different grain size ranges, closely resembling the ones at the drilling site, were selected for preparing the synthetic mixtures in the laboratory. For these sand grains, the mean diameter (D_{50}) for particle sizes of 0.425–1.4 mm (termed as "coarse") was 0.56 mm and, for grain sizes of 0.125–0.355 mm (termed as "fine"), was 0.20 mm. The coefficient of uniformity ($C_u = D_{60}/D_{10}$) for the coarse and fine sand grains was 1.452 and 2.268, respectively. The sands were sieved and packed into plastic bags, about 3 kg in each, to preserve the natural moisture content of the sands. The density of the fine and coarse sand particles was 1.47 g/cm^3 and 1.59 g/cm^3, respectively.

4.3. Water content

According to Gueguen and Palciauskas (1992), water content should be kept at a minimum value to avoid segregation of the cement and sand grains. Different water contents were considered to create the most suitable mixture. To determine the optimum water content for the mixture, standard Proctor compaction tests were conducted (Fig. 5). These tests were performed on mixtures both with and without cement. Fig. 5 shows that the optimum water ratio evaluated by using compactor hammer with energy of 0.55 N m/cm^3 was achieved at 9.7%–10.3%. There was no significant change in optimum water content and density in the case of the sand and cement mixture or of the sand grains only.

4.4. Cement content

Portland cement type II (specific gravity $G_s = 3.15$) was used for preparing the TWHC specimens based on previous studies on the mechanical properties of weakly cemented sands (Saidi et al., 2003). The cement powder used in the current study was from a single bag and it was kept in a sealed and airtight container throughout the laboratory studies.

For preparing poorly cemented sands in laboratory conditions, a wide range of w_c values have been suggested by different researchers (Alsayed, 1996; Kongsukprasert, 2003; Saidi et al., 2003, 2005). Kongsukprasert (2003) used a maximum of 2.5% of Portland cement, whereas Saidi et al. (2003) used 9%–18%. In addition, Gueguen and Palciauskas (1992) stated that the minimum w_c is reached when the coarse-to-fine sand particle ratio, δ, is equal to 1.5. Saidi et al. (2005) showed that a very small amount of Portland cement will increase the strength and stiffness of cemented sand mixtures if deposited at grain-to-grain contacts. However, based on the authors' observations, using sands of the above-mentioned grain size distribution, for $w_c \leq 2.5\%$, the specimens could not be successfully de-moulded after the curing time (2–12 days).

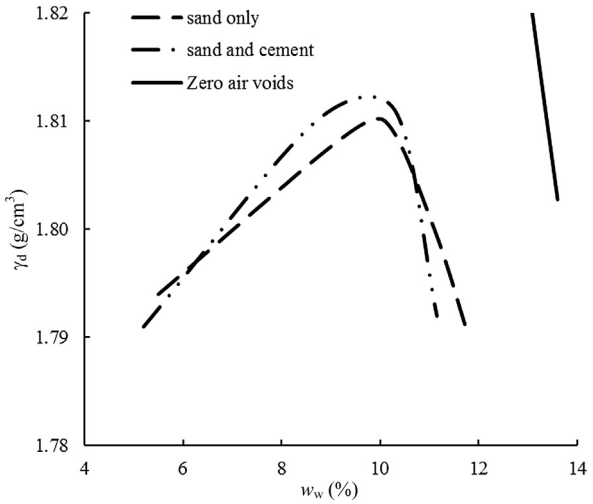

Fig. 5. Proctor compaction test results of silica sand with and without Portland cement powder ($w_c = 6\%$). γ_d is the dry density (g/cm^3), and w_w is the water content (%).

A number of mixtures with different values of w_c and δ were prepared and examined to achieve the apparent mechanical behaviour of the drilling site samples. For the mentioned particle size distribution range, values of $w_c = 6\%$, 7% and 8% were selected. According to the test results, since the grain size distribution significantly affects the strength of the specimens, it is not possible to create poorly cemented sand samples by using a fixed w_c value for different particle size distributions.

4.5. Coarse-to-fine sand particle ratio (δ)

The cement content, w_c, and the coarse-to-fine sand particle ratio, δ, were varied to obtain the desirable mixture. In this study, since the cement powder particle is finer than the sand grains, the cured Portland cement is assumed to be a continuous phase despite the fact that it includes micro-granule and micro-porosity (Saidi et al., 2005). The specimen contains three separate phases: sand, cement and macro-porosity larger than the sand grain size (Ashby and Jones, 2014). Scanning electron microscope (SEM) photographs confirmed that macro-porosities were often larger in size than the sand particles themselves (Fig. 6a). According to Saidi et al. (2005), the minimum macro-porosity is achieved when δ is around 1–3. Also, based on the collected samples from the drilling site, the cured mixture should be weak enough to allow sand particles to debond when the surface is scratched with a finger nail. Therefore, different values of δ were examined for a constant w_c to determine the most suitable δ. Finally, $\delta = 1$ was chosen based on the test outcomes which are discussed later.

4.6. Curing time

Various curing times have been suggested in previous studies (e.g. Kongsukprasert, 2003; Saidi et al., 2003). In the current research, curing times of 2–12 days were examined. The curing time includes the curing of the mixture, both in the mould and after de-moulding. In the case of less than 5 days curing, the specimens

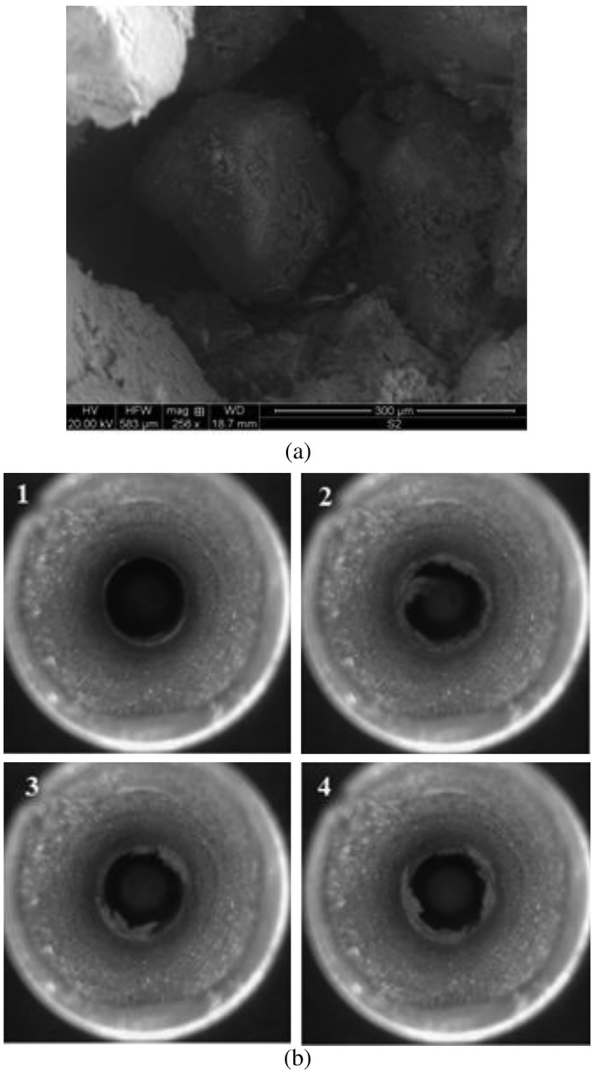

(a)

(b)

Fig. 6. (a) SEM photograph showing that macro-porosities are larger than sand particles in the cemented sand mixture. (b) Borehole breakout occurring in the area which seems to still contain some moisture.

could not be successfully de-moulded. Preliminary tests were performed on TWHC specimens with total 5 days curing time. Careful examination of the video taken during testing and of the cross-sections of the tested specimens (Fig. 6b) revealed that all boreholes had failed in a zone that seemed to have retained some moisture and had not yet completely dried. After further studies, based on the uniaxial compressive strength (UCS) test results, 5-day curing was deemed to be the optimal time for curing inside the mould when the specimen was compacted at atmospheric pressure. After removal of the mould, each specimen was wrapped by plastic film, placed in an airtight plastic container and left to further curing for another 3 days under atmospheric pressure and at a constant water content. To ensure that 26%–29% porosity was achieved, no external pressure was applied to the specimens whilst curing.

5. Results and discussion

In order to determine the properties of the mixture, various preliminary tests were conducted on solid and TWHC specimens. The results of these tests can be used to compare other drilling fields and ground conditions to those examined in the current study. Preparation of the mixture began with $w_c = 1\%$ using only fine grained sands. Table 1 presents the details of the physico-mechanical properties that were observed from the uniaxial and triaxial tests. To determine the mechanical properties of the specimens, a number of solid cylindrical specimens with different sand grain size distributions, Portland cement and water contents were prepared.

Table 1
Properties of the prepared poorly cemented sand specimens.

w_c (%)	Porosity, n (%)	Tangent elastic modulus, E_{tan} (GPa)	UCS (MPa)	Poisson's ratio, ν	Coulomb parameters		Bulk density, ρ (kg m^{-3})
					c (MPa)	ϕ (°)	
6	26 ± 3	2.262	0.62	0.294	1.11	29.67	1954
7	26 ± 2	2.465	1.05	0.250	1.38	30.06	1969
8	26 ± 2	3.360	1.90	0.247	1.59	29.67	1974

5.1. Effect of coating on the strength of TWHC specimens

Based on the preliminary test results, foil strain gauges and external LVDTs were selected to measure the axial and lateral strains during triaxial testing. To identify the most suitable coating for poorly cemented sands, three specimens with the same characteristics were prepared. Four strain gauges were placed on each specimen with different underlining conditions (i.e. polymer, plastic bond, no lining). The results from the strain gauges using the plastic bond lining and the specimen without lining showed irregularities in the stress–strain diagrams, but the strain gauges placed on the polymer coating showed good and reproducible results and the cohesion of the polymer and specimen continued to be preserved after the test. Thus, polymer coating was deemed to be the best suited option for the subsequent triaxial testing.

In addition, the strengthening effect of the polymer on the poorly cemented sand TWHC specimens was considered. Video recordings that were taken inside the borehole of the preliminary TWHC tests showed that the debonding of sand particles in the specimens initiated in the zone out of the applied polymer location (e.g. top and bottom sections of the borehole, see Fig. 7a). In the tests without coating, debonding often began uniformly in the middle of the specimens. However, using polymer coating is essential for obtaining accurate readings from the strain gauges, as discussed earlier. To address this problem, in subsequent tests a thin layer of polymer was applied along the length of all the specimens symmetrically as is shown in Fig. 7b. The results showed the significance of using the camera in identifying the factors affecting the process of sand debonding from the borehole wall.

5.2. UCS tests on solid specimens

5.2.1. Effect of particle size distribution in UCS tests

As mentioned above, two sets of sands, namely fine (0.125–0.355 mm) and coarse (0.425–1.4 mm) grained sands, were examined in this study. Three sets of UCS tests were performed on solid specimens with the same values of $w_c = 8\%$ and $w_w = 10\%$, but with different coarse-to-fine sand particle ratios (δ) (i.e. 0.14, 0.33 and 1). The specimens were left to curing for 5 days at atmospheric pressure with the same curing method that was discussed earlier in Section 4.6.

Fig. 8a shows that the influence of δ on the peak strength and pre-peak stiffness is considerable. It is evident that, whilst maintaining w_c constant (i.e. at 8%), the strength and stiffness of the specimens increase as the proportion of coarse sand particles (i.e. δ)

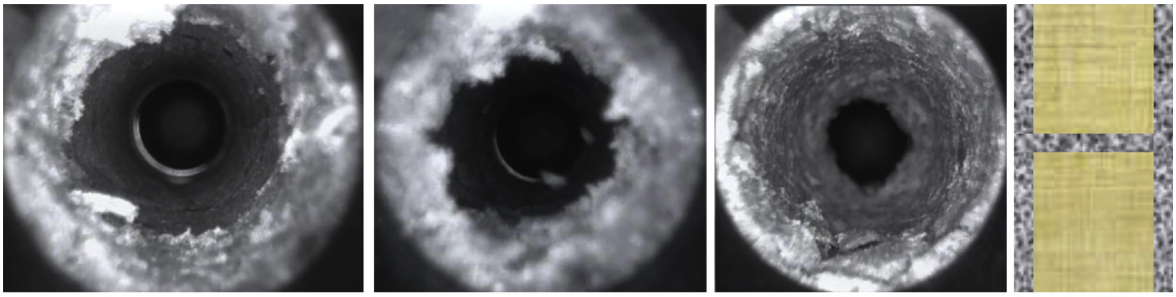

Fig. 7. (a) Borehole breakout occurring in an area out of strain gauge coating; and (b) polymer application pattern to minimise the effect of coating on the strength of the specimens.

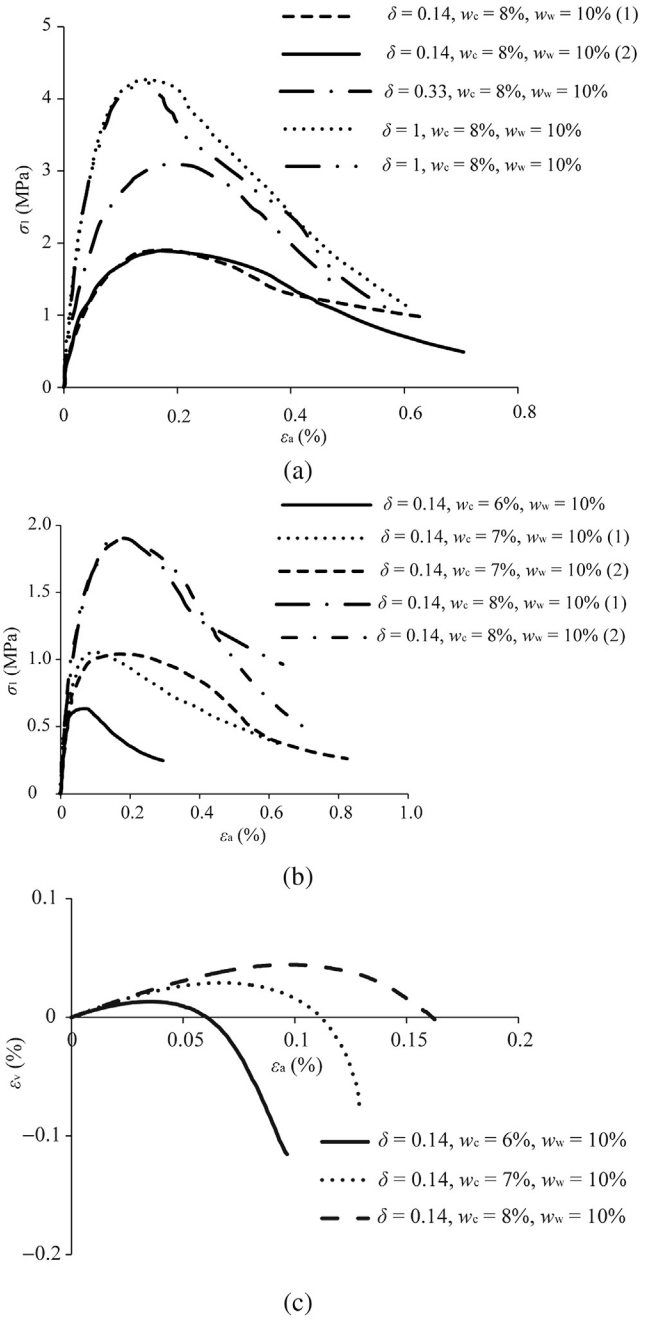

Fig. 8. Results of UCS tests. (a) Effect of different δ values on the strength of poorly cemented sand specimens; (b) Effect of different w_c values on the stress–strain diagrams and (c) on the volumetric strain, where ε_a is the axial strain.

rises and the specimens become more brittle in the post-peak regime. The strength of the mixture increases significantly as δ grows because the coarse sand particles exhibit greater resistance to rotation in the specimen matrix than the fine particles. Therefore, when the number of the coarse grains increases, the rotation of particles becomes more difficult due to the improved level of interlocking between the particles after compaction and the global compressive strength of the mixture is increased. In the case of higher δ, the other reason behind the mixture strength growth is the decrease in the special surface of sand particles in the whole matrix which enhances the influence of cementation in the specimen. Therefore, by increasing the sand grain size, it is possible to obtain a higher strength mixture for a certain w_c value. This confirms the findings by other researchers (Kongsukprasert, 2003; Saidi et al., 2003, 2005) who used different ranges of w_c to create cemented sand specimens. Also, the level of compaction improved with the increase of δ up to a certain level and thus the cementing agent could bond more sand particles in a unit volume.

It should be noted that increasing δ by more than 1 was not considered in this research, because the aim was to test particle sizes similar to those observed at the Burra drilling site.

5.2.2. *Effect of cement content in UCS tests*

To study the effect of cement content (w_c), three different values of w_c were considered, namely 6%, 7% and 8% under the same testing conditions. To examine reproducibility of the results, specimens with 7% and 8% of cement content were tested twice. Fig. 8b presents the stress–strain diagrams of the specimens with a dry density of 1.81 g/cm^3 after 7 days curing.

From the UCS test results, the following trends can be observed:

(1) The maximum strength, σ_{max}, and pre-maximum stiffness increase as w_c rises. This outcome is in agreement with Saidi et al. (2003) and Kongsukprasert et al. (2005) who used other ranges for w_c and δ.
(2) The post-peak stress–strain trend of the specimens with lower values of w_c exhibits greater ductile behaviour. As shown in Fig. 8a and b, the UCS is affected to a greater extent by w_c than δ.

The effect of w_c on the volumetric strain is presented in Fig. 8c. It can be observed that as w_c increases the specimens experience greater axial and volumetric strains prior to failure. In addition, for lower w_c values, dilation is evident in the specimens after a limited amount of compression. However, with increasing cementation the lateral strain decreases and the volumetric strain is affected mostly by the axial compression strain. The axial strain increased by about 83% and 84% at $\varepsilon_v = 0$ with w_c increasing from 6% to 7% and from 7% to 8%, respectively.

Furthermore, the effect of water required for cement hydration was considered by increasing the water content in small

increments within the range of 5%–12%, covering the dry, optimum, and wet sections of the optimum water diagram. Kongsukprasert et al. (2005) showed that, for the cemented sand mixture, the added water cannot be entirely used for cement hydration. The total water content of the mixture comprises of a part that serves to hydrate the cement and another part is absorbed by the grains at the time when water is added to the mixture. In addition, Chen and Wu (2013) suggested that the degree of hydration increases as the curing time and water-to-cement ratio of the mixture rise. However, they showed that excessive water content increases the total porosity and results in strength reduction. When the sand grains are not in the saturated-surface dry (SSD) mode, part of the water will be absorbed by the grains, while the remaining part covers the particles' surfaces. Specimens with less than 6% water content could not be de-moulded after even 10 and 12 days of curing time, which inferred that, due to the high specific surface of the sand particles, a minimum of 6% water content was required to achieve hydration. The results showed that, for a specific density of a compacted mixture, the highest strength is obtained with the water content at or around the optimum one, and the strength is significantly reduced when the water content is less than the optimum value. As mentioned earlier, the optimum water content was determined by standard compaction tests and was found to be almost 10%.

5.3. Triaxial test results on solid specimens

Triaxial tests on solid specimens were performed to determine the shear failure properties of the specimens under different stress conditions. Table 2 shows a summary of the final values of δ, w_c and w_w which were identified by preliminary tests, where σ_{conf} is the confining pressure.

Fig. 9a–c presents the results of the triaxial tests on the solid specimens with different w_c values. As shown in Fig. 9, an increase in confining pressure results in an increase in peak strength. However, the confining pressure has a minimal effect on the stiffness of the specimens. Also, as it can be seen from Fig. 9, this material exhibits strain hardening behaviour, i.e. continuous increase in the deviatoric stress with axial strain. Thus, the stress corresponding to 1% of axial strain was considered as the maximum strength of the specimens. The results show that the material behaves nonlinearly even in the early stages of the loading process as was seen by the UCS tests earlier. Paterson (1967) showed that ductility increases with increasing σ_3. Fig. 9 shows that the ductility of the specimens at lower confining pressures is less significant and increasing the confining pressure results in the transition from brittle to ductile behaviour. According to the results, for w_c = 7% and 8%, the elastic strain remains relatively constant due to an increase in confining pressure. Higher confining pressures (e.g. >6–6.5 MPa) were examined for specimens in each of the three categories and the results showed that strain gauges on the specimens failed at these higher confining pressures. This problem often occurs due to the sandy surface and weak matrix of this material.

Table 2
Schedule of the triaxial tests conducted on solid and poorly cemented TWHC sand specimens.

Type of specimens	w_c (%)	δ	Borehole size (mm)	σ_{conf} (MPa)	Displacement rate (mm/min)	w_w (%)	Curing time (d)
Solid cylinder	6, 7, 8	1	–	1–5	0.07	10	8
TWHC	6, 7, 8	1	10, 20	1–5	0.07	10	8

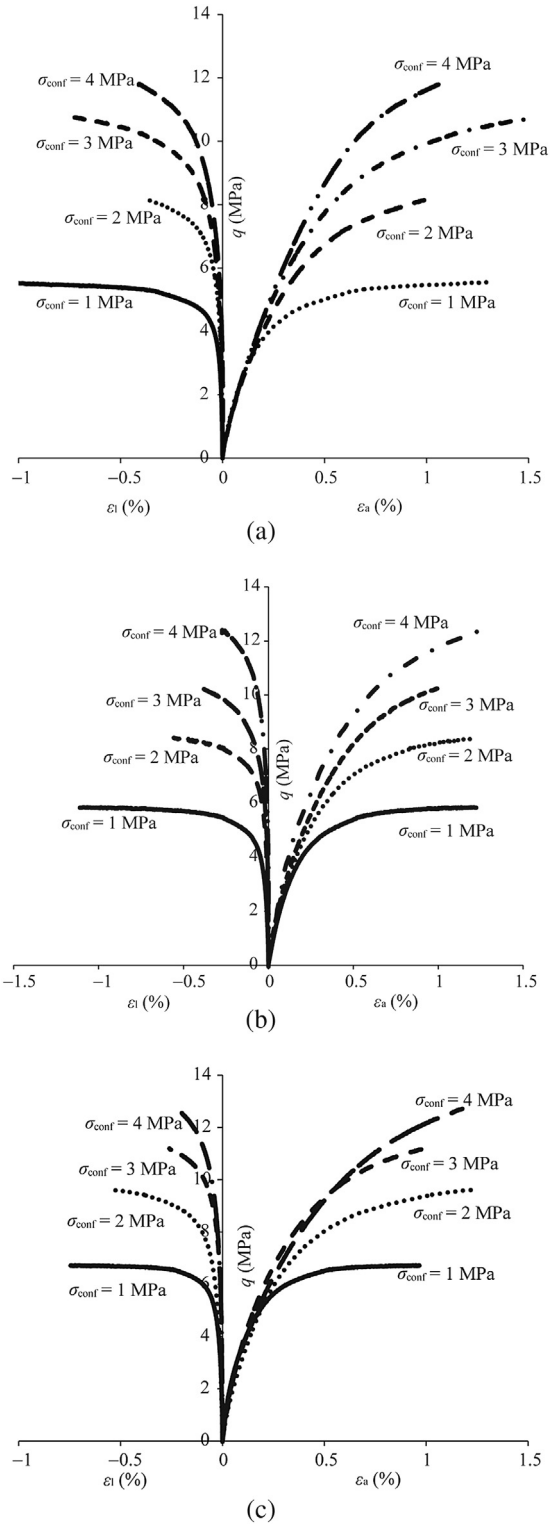

Fig. 9. Deviatoric stress versus axial and lateral strain behaviours of solid specimens subjected to triaxial testing: (a) w_c = 6%; (b) w_c = 7%; and (c) w_c = 8%.

5.3.1. Mohr–Coulomb strength parameters

Mohr–Coulomb criterion is one of the most commonly used failure criteria in borehole stability problems (Jaeger et al., 2007). Coulomb suggested that shear failure will take place when the shear stress is equal to the sum of cohesive shear strength and the product of the coefficient of internal friction and normal stress

across the fracture plane. Later, Mohr asserted that the relationship between the normal and shear stresses along the failure plane is nonlinear:

$$\tau = f(\sigma_n) \tag{4}$$

where f is a function that can be derived empirically.

To explain the behaviour of the material by the Coulomb failure criterion, the cohesion, c, and the angle of internal friction, ϕ, were determined. As expected, increasing the cement content produces higher cohesion between the sand grains, and based on the Mohr–Coulomb criterion, c (cohesion) changes for different cement values. The c and ϕ values are presented in Table 1. For different w_c values, the derived ϕ values show that the angle of internal friction does not change dramatically due to the increase in the cement content. This is mainly due to the grain size distribution not being changed in the specimens tested.

5.3.2. Volumetric strain results

Lateral strain was measured during the triaxial tests on solid specimens to study the effect of confining pressure and cement content on the volumetric strain of the prepared specimens. Fig. 10 shows the average values of the volumetric strains calculated based on average values of lateral and axial strain gauges for solid and TWHC specimens. As can be seen in this figure, at lower confining pressures (i.e. 1 MPa and 2 MPa) the solid specimens began to contract from the top and bottom sections first and after 0.55% axial compression strain, it diverted to lateral dilation. Increasing the confining pressure kept the specimen in a more contraction mode and dilation began at higher axial strain values. With an increase in the confining pressure, the lateral strength of the specimens will rise and the lateral dilation will be lower for the same axial strain. As mentioned earlier, after the elastic phase in the stress–strain diagram, the solid specimens exhibited strain hardening behaviour. Thus, for confining pressures greater than 2 MPa, the solid specimens remained in contraction mode and never conjugated the horizontal axis (i.e. the zero volumetric strain) until the maximum strength which was assumed equivalent to 1% of axial strain. The results also show that the effect of varying the cement contents on the volumetric strain is less significant than altering the confining pressure. For instance, at confining pressures of 1 MPa and 2 MPa, increasing the w_c value from 6% to 8% does not result in any divergence in the behavioural trend from contraction to dilation in the specimens.

Fig. 9 also presents the deviatoric stress versus lateral strain behaviour for solid specimens. It shows that applying higher confining pressure slightly increases the stiffness of the material in the lateral direction. In addition, the specimens exhibited more brittle behaviour at low confining pressures and, with increasing confining pressure, the material response became more ductile. It is worth mentioning that the specimens underwent lower lateral deformation by increasing the w_c value at a constant w_w, δ and confining pressure.

5.4. Triaxial test results on TWHC specimens

Triaxial tests on TWHC specimens were conducted to investigate the borehole breakout and failure properties of the synthetic specimens under different stress conditions. Real-time video recording helped to determine the initiation and direction of borehole breakout and to locate the sand debonding on the borehole wall. The main TWHC tests were conducted for three different cement contents (w_c) and for two different borehole diameters: 10 mm and 20 mm.

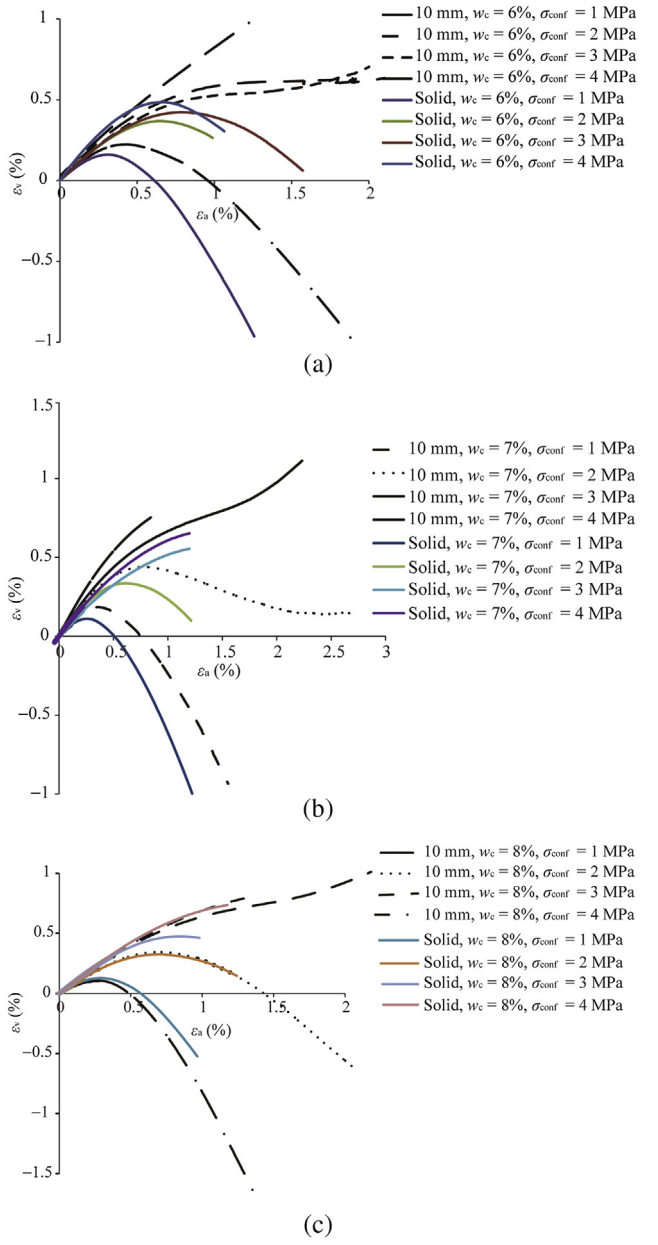

Fig. 10. Volumetric strain versus axial strain results from triaxial tests on solid and TWHC (10 mm borehole) specimens: (a) $w_c = 6\%$; (b) $w_c = 7\%$; and (c) $w_c = 8\%$.

Fig. 11 presents the results of the triaxial tests on 10 mm diameter borehole TWHC specimens for three different w_c values (6%, 7% and 8%) and various confining pressures. As shown in Fig. 11a, increasing the confining pressure from 1 MPa to 3 MPa significantly enhances the level of peak strength and strain energy in the specimens. It should be mentioned that the pre-peak stiffness does not change dramatically with an increase in the confining pressure for a certain w_c. However, for $\sigma_{conf} > 3$ MPa, the level of the strength increment is lower than that for the previous states. For confining pressures higher than 4.5 MPa, the first stage of the test (i.e. applying hydrostatic stress to the boundary of the specimens) could not be completed and the borehole collapsed immediately.

Fig. 12 shows the process of the borehole failure prior to applying the deviatoric stress. However, the axial strain gauges continued to function even after failure. This emphasises the significance of using the micro-camera during the borehole stability studies.

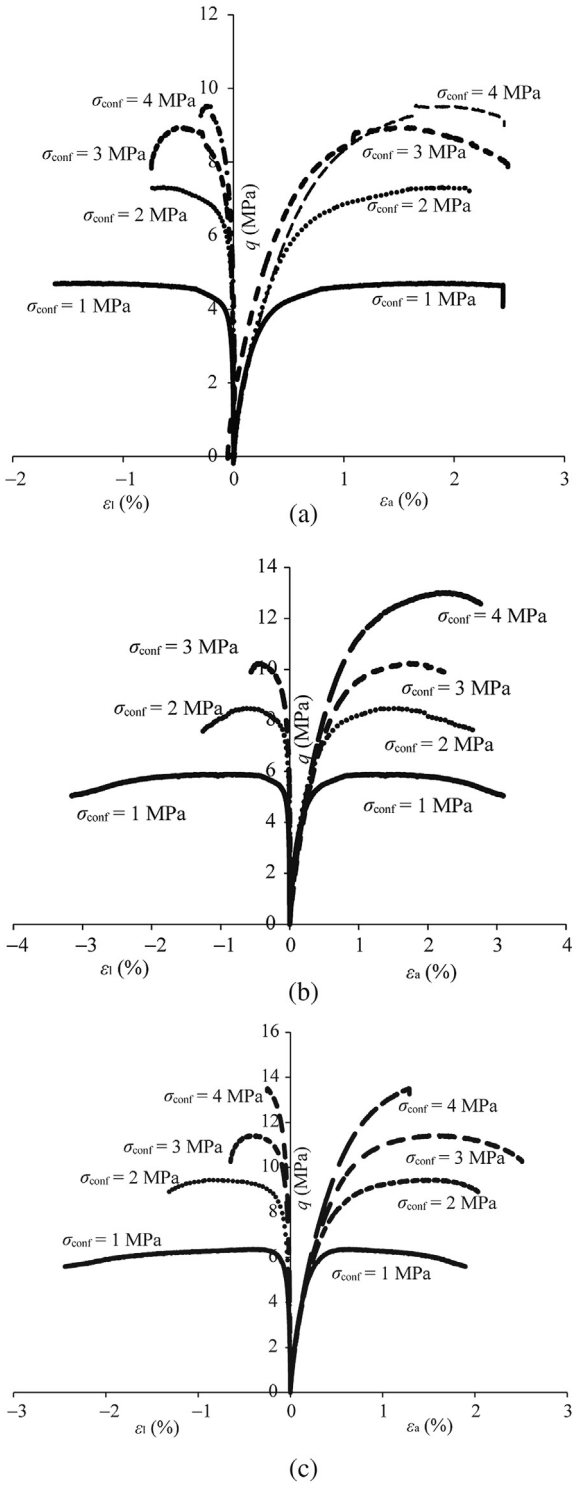

Fig. 11. Deviatoric stress versus axial and lateral strain behaviours of 10 mm borehole TWHC specimens for (a) $w_c = 6\%$, (b) $w_c = 7\%$, and (c) $w_c = 8\%$, and the effect of the confining pressure on the strength of the specimens.

As shown in Fig. 13a, unlike the solid specimen test results, the TWHC specimens did not exhibit strain hardening behaviour after the maximum strength and the peak strength can be determined in the applied stress ranges. Fig. 13a shows that the ductility of the specimens increases with an increase in the confining pressure as is the case for the solid specimens.

Also, increasing the cement content by a small amount slightly increases the stiffness of the specimens for the same sample preparation and test condition.

The results show that the confining pressure has a minimal effect on the stiffness as exhibited in the stress–strain curves. This result agrees with that of Mogi (2007) who showed that the yielding stress of ductile rocks does not increase with increasing confining pressure.

5.4.1. *Effect of w_c and σ_{conf} on lateral and volumetric strains*

Fig. 11 also shows the deviatoric stress versus the average lateral strain for different values of w_c and confining pressures. Analysis of the micro-camera video recordings and Fig. 11 show that, for a given w_c, with an increase in the confining pressure, the borehole breakout initiates at a lower lateral strain and the ductility in the direction of σ_{conf} decreases. However, as mentioned in the previous section, increasing the confining pressure results in greater ductility.

Fig. 10 also shows that, at lower confining pressures (i.e. 1 MPa and 2 MPa), the TWHC specimens transit to the dilation mode and with an increase in the confining pressure the borehole breakout initiates in a contraction mode as in solid specimens. This is mainly due to the fact that high confining pressures create borehole convergence and therefore the size of the sample in the lateral direction reduces. Also, due to the presence of a borehole at low confining pressure, the volumetric strain curve conjugates the horizontal axis at higher axial strain value in comparison with solid specimens in the same confining pressure, suggesting that microcracks are developing on the borehole wall and sand grain dislocation occurs in the TWHC specimens versus solid specimens to release the applied stresses and return the equilibrium condition to the specimen. In addition, as shown in Fig. 10a–c, with an increase in w_c, the lateral strain increases compared to the axial strain and prior to borehole breakout in the TWHC specimen, axial contraction of specimens with higher w_c is less than that of the specimens with lower cement content. In other words, an increase in w_c results in decrease in the pore spaces of the specimens, and application of the axial deviatoric stress causes less contraction in the axial direction. Therefore, for higher w_c values, the lateral strain of poorly cemented sand specimens is more dominant in comparison with the axial contraction. Based on the real-time camera recordings, it can be stated that, in the samples where dilation failure happened, the transition from the volumetric strain contraction to the dilation occurred before the borehole breakout initiation. Also for the same specimen condition, increasing the cement value by a small amount slightly increases the stiffness of the specimens under a certain confining pressure (Fig. 13b).

5.4.2. *Size-scale effect on TWHC specimens*

As mentioned above, the TWHC specimens were prepared in two borehole sizes: 10 mm and 20 mm. The same process was adopted for the 20 mm borehole specimens, including grain size distribution, curing time, compaction force, and so on. Triaxial tests were performed on 20 mm borehole specimens for different w_c values and confining pressures. Fig. 14a presents the deviatoric stress versus the axial and lateral strains for 20 mm borehole TWHC specimens for $w_c = 7\%$ and different confining pressures. Fig. 14b illustrates the results of the specimens with 10 mm and 20 mm borehole sizes to compare their behaviours. As expected, the strength of the 20 mm borehole TWHC specimens at failure is generally lower than that of the smaller borehole specimens especially at higher confining pressures due to size-scale effect which was shown by Carpinteri (2002). Also, it shows a considerable decrease in ductility for the 20 mm borehole specimens versus that for the specimen with a 10 mm borehole. Fig. 14b shows that

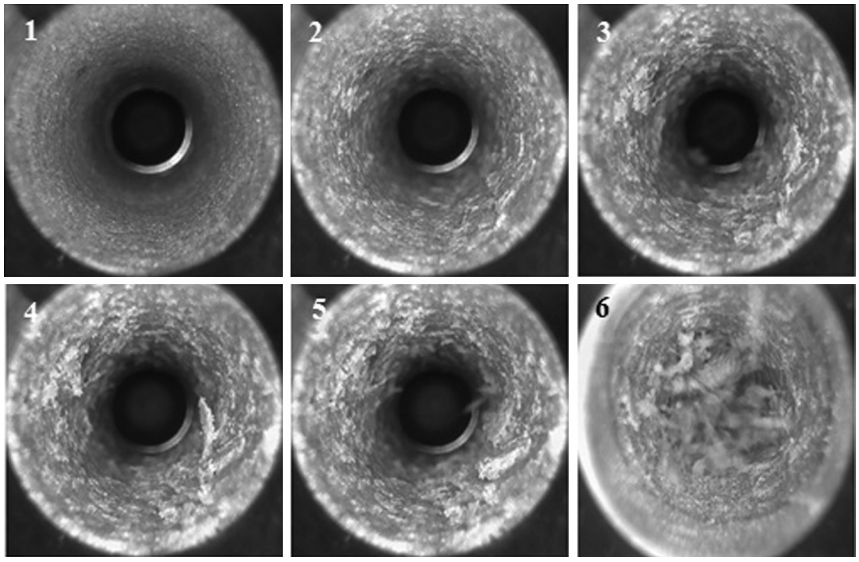

Fig. 12. Sand dislocation and borehole collapse processes due to the hydrostatic pressure with high confining pressure (6 MPa) prior to the application of the deviatoric stress to the TWHC specimen.

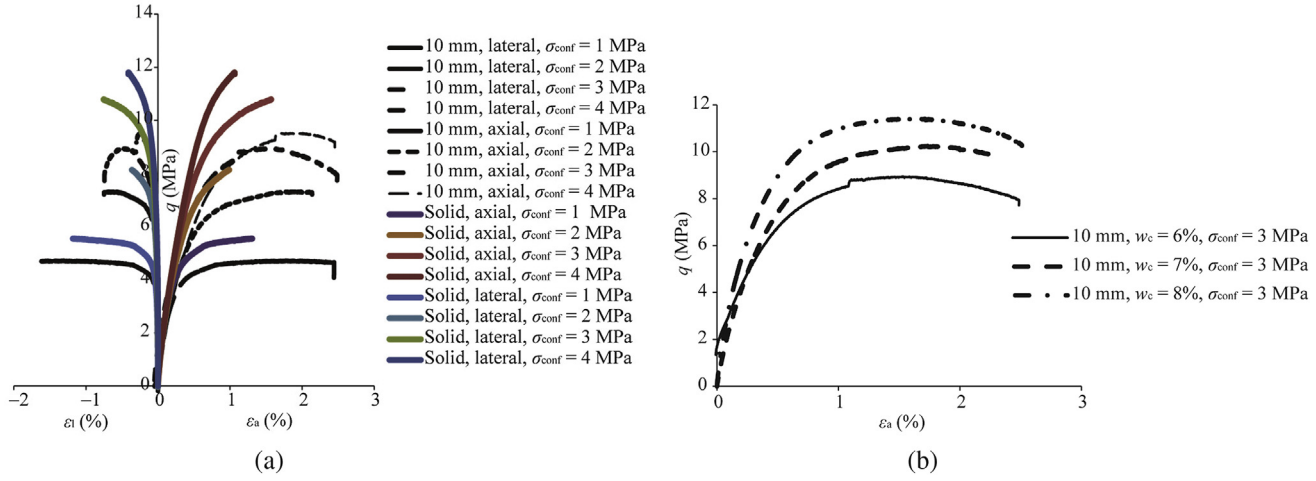

Fig. 13. (a) Diagram comparing stress–strain behaviour of 10 mm borehole TWHC and solid specimens for $w_c = 6\%$; and (b) Effect of cement content on the strength of the TWHC specimens for a given confining pressure ($\sigma_{conf} = 3$ MPa).

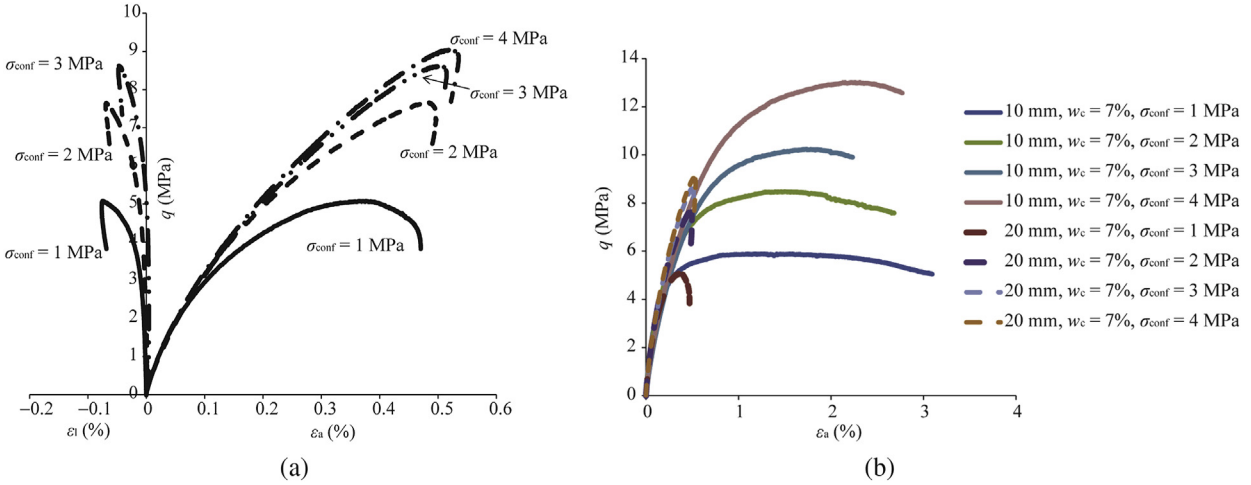

Fig. 14. (a) Deviatoric stress versus axial and lateral strains of 20 mm borehole TWHC specimens for $w_c = 7\%$; and (b) Diagram comparing stress–strain behaviours of 10 mm and 20 mm borehole specimens for $w_c = 7\%$.

the stiffness of the TWHC specimens does not change with increasing borehole size. This is in agreement with Mogi (2007) who suggested that the stiffness depends on the rock material and, since the same mixtures were used for both specimens with different borehole sizes, the same stiffness was observed from the tests.

In lateral direction, Fig. 14a shows that with increasing confining pressure, the lateral strain decreases for specimens with 20 mm borehole and the same w_c values. In addition, it was observed that under different confining pressures the lateral strain at the borehole breakout initiation point is considerably lower in the 20 mm borehole specimens when compared with the 10 mm borehole specimens (see also Fig. 11b). However, the lateral stiffness remains unchanged and is unaffected by the increase in borehole size from 10 mm to 20 mm. Also, the lateral ductility significantly decreased in the specimens of larger borehole size. In other words, the breakout in the borehole with larger diameter (20 mm) occurred at a lower strain compared to that for a smaller diameter borehole (10 mm).

6. Conclusions

This study has examined the stability of boreholes in poorly cemented sand by a series of newly developed laboratory tests. It was observed that the strength of the poorly cemented sand specimens is largely influenced by the mould conditions. The real-time monitoring of preliminary tests on TWHC specimens showed that in the case of curing the specimens for less than 8 days ($w_w = 10\%$), borehole breakout initiated in a zone which was not fully dry. At a given w_c, the peak strength and stiffness of the specimens increased with an increase in the weight of coarse sand grains. Also, the specimens showed more brittle behaviour for higher levels of δ.

The post-peak stress–strain behaviour of the specimens with lower w_c showed more ductile trend and the effect of w_c was more considerable than that of δ in the UCS tests. In lower w_c values, dilation occurred after a limited compression in the specimens and with the increasing cementation the lateral strain decreased and the volumetric strain was mostly dominated by the axial compression strain.

Using the videos recorded during the preliminary test on TWHC specimens, the strengthening effect of the applied coating was investigated and it was found that the borehole breakout started in the area out of the section where polymer was applied.

Solid specimens exhibited strain hardening behaviour and no peak strength was observed in their stress–strain diagram both in axial and lateral directions. Unlike the solid specimens, TWHC specimens did not exhibit strain hardening behaviour after the maximum strength was reached and the peak strength could be determined in the applied stress ranges.

At lower confining pressures (i.e. 1 MPa and 2 MPa), solid specimens started contracting initially from the top and bottom sections and after 0.5%–0.6% of axial compression strain, it diverted to the lateral dilation. Increasing the confining pressure kept the specimen in contraction mode and dilation started with delay at a higher axial strain. For confining pressures of more than 2 MPa, specimens remained in contraction mode and never diverted to the dilatation until the maximum strength was reached.

For the TWHC specimens with confining pressures higher than 4.5 MPa, the first stage of the test could not be completed and the borehole failed before the application of the deviatoric stress. Also, in the TWHC specimens the volumetric strain curve conjugated the axial strain axis at a higher magnitude which suggested that micro-cracks were formed on the borehole wall and sand grain dislocation took place in TWHC versus solid specimens to release the applied stresses. Based on the observations from the real-time camera recording, it can be stated that the transition from the volumetric strain contraction to the dilation occurred before the initiation of borehole breakout.

The failure strength of the 20 mm borehole TWHC specimens was less than that of the 10 mm ones especially at higher confining pressures due to the size-scale effect. Also, ductility was less in 20 mm borehole specimens in comparison with that in the 10 mm ones. However, the stiffness in axial and lateral directions did not change with an increase in the borehole size. Also, it was observed that the lateral ductility significantly decreased in the specimens with larger borehole size.

For further investigation on the behaviour of poorly cemented sands, it is suggested to upgrade the laboratory tests to polyaxial stress condition in order to simulate anisotropic horizontal in-situ stresses adjacent to a drilled borehole.

Conflict of interest

The authors wish to confirm that there are no known conflicts of interest associated with this publication and there has been no significant financial support for this work that could have influenced its outcome.

Acknowledgements

This work has been supported by the Deep Exploration Technologies Cooperative Research Centre whose activities are funded by the Australian Government's Research Programme. This is DET CRC Document 2015/262.

References

Adeyanju OA, Olafuyi OA. Experimental studies of sand production from unconsolidated sandstone petroleum reservoirs in Niger-Delta. Nigerian Journal of Technology 2011;30(2):18–30.
Al-Ajmi AM, Zimmerman RW. Stability analysis of vertical boreholes using the Mogi–Coulomb failure criterion. International Journal of Rock Mechanics and Mining Sciences 2006;43(8):1200–11.
Al-Awad MNJ, El-Sayed AH, Desouky SEM. Factors affecting sand production from unconsolidated sandstone Saudi oil and gas reservoir. Journal of King Saud University, Engineering Sciences 1999;11(1):151–74.
Alsayed MI. Rock behaviour under multiaxial compression. PhD Thesis. Newcastle, UK: University of Newcastle upon Tyne; 1996.
Ashby MF, Jones DRH. Engineering materials 2: an introduction to microstructures, processing and design. Elsevier; 2014.
Bridgman PW. Studies in large plastic flow and fracture with special emphasis on the effects of hydrostatic pressure. New York-London: McGraw-Hill; 1952.
Carpinteri A. Size-scale effects in the failure mechanisms of materials and structures. CRC Press; 2002.
Chang C, Moos D, Zoback MD. Anelasticity and dispersion in dry unconsolidated sands. International Journal of Rock Mechanics and Mining Sciences 1997;34(3–4):48.e1–48.e12.
Chen X, Wu S. Influence of water-to-cement ratio and curing period on pore structure of cement mortar. Construction and Building Materials 2013;38:804–12.
Cleary MP, Melvan JJ, Kohlhaas CA. The effect of confining stress and fluid properties on arch stability in unconsolidated sands. In: SPE Annual Technical Conference and Exhibition. Las Vegas; 1979. Nevada, SPE 8426.
Ewy R, Cook NGW. Deformation and fracture around cylindrical openings in rock—I. Observations and analysis of deformations. International Journal of Rock Mechanics and Mining Sciences & Geomechanics Abstracts 1990a;27(5):387–407.
Ewy R, Cook NGW. Deformation and fracture around cylindrical openings in rock—II. Initiation, growth and interaction of fractures. International Journal of Rock Mechanics and Mining Sciences & Geomechanics Abstracts 1990b;27(5):407–27.
Ewy RT, Cook NGW, Myer LR. Hollow cylinder tests for studying fracture around underground openings. In: Proceedings of the 29th US Symposium on Rock Mechanics (USRMS). Minneapolis, MN: American Rock Mechanics Association; 1988.
Fischer PW, Pye, DS, Gallus JP. Method for drilling a well through unconsolidated dolomite formations. Patent US4120369; 1978.
Geertsma J. Some rock-mechanical aspects of oil and gas well completions. Society of Petroleum Engineers Journal 1985;25(6):848–56.

Gough D, Bell J. Stress orientations from borehole wall fractures with examples from Colorado, east Texas, and northern Canada. Canadian Journal of Earth Sciences 1982;19(7):1358–70.
Gueguen Y, Palciauskas V. Introduction à la physique des roches. Hermann. 1992 (in French).
Hagin PN, Zoback MD. Viscous deformation of unconsolidated reservoir sands. Part 1: time-dependent deformation, frequency dispersion, and attenuation. Geophysics 2004;69(3):731–41.
Haimson BC, Song I. Laboratory study of borehole breakouts in Cordova Cream: a case of shear failure mechanism. International Journal of Rock Mechanics and Mining Sciences & Geomechanics Abstracts 1993;30(7):1047–56.
Hall JCD, Harrisberger WH. Stability of sand arches: a key to sand control. Journal of Petroleum Technology 1970;22(7):821–9.
Hashemi SS, Momeni AA, Melkoumian N. Investigation of borehole stability in poorly cemented granular formations by discrete element method. Journal of Petroleum Science and Engineering 2014a;113:23–35.
Hashemi SS, Taheri A, Melkoumian N. Shear failure analysis of a shallow depth unsupported borehole drilled through poorly cemented granular rock. Engineering Geology 2014b;183:39–52.
Hoskins ER. The failure of thick-walled hollow cylinders of isotropic rock. International Journal of Rock Mechanics and Mining Sciences & Geomechanics Abstracts 1969;6(1):99–125.
Jaeger JC, Cook NGW, Zimmerman RW. Fundamentals of rock mechanics. John Wiley & Sons Inc.; 2007.
King LV. On the limiting strength of rocks under conditions of stress existing in the earth's interior. The Journal of Geology 1912;20(2):119–38.
Kongsukprasert L. Time effects on the strength and deformation characteristics of cement-mixed gravel. PhD Thesis. Tokyo, Japan: University of Tokyo; 2003.
Kongsukprasert L, Tatsuoka F, Tateyama M. Several factors affecting the strength and deformation characteristics of cement-mixed gravel. Soils and Foundations 2005;45(3):107–24.
Lee M, Haimson B. Laboratory study of borehole breakouts in Lac du Bonnet granite: a case of extensile failure mechanism. International Journal of Rock Mechanics and Mining Sciences & Geomechanics Abstracts 1993;30(7):1039–45.
Mazanti B, Sowers G. Laboratory testing of rock strength. In: STP402: testing techniques for rock mechanics. ASTM; 1966. p. 207–27.
Mogi K. Experimental rock mechanics. CRC Press; 2007.
Obert L, Duvall WI. Rock mechanics and the design of structures in rock. New York: John Wiley & Sons Inc.; 1967.
Paterson MS. Effect of pressure on stress-strain properties of materials. Geophysical Journal International 1967;14(1–4):13–7.
Perkins TK, Weingarten JS. Stability and failure of spherical cavities in unconsolidated sand and weakly consolidated rock. SPE18244. 1988.
Pomeroy CD, Hobbs DW. The fracture of coal specimens subjected to complex stresses. Steel and Coal 1962;185:1124–33.
Robertson EC. Experimental study of the strength of rocks. Geological Society of America Bulletin 1955;66(10):1275–314.
Saidi F, Bernabé Y, Reuschlé T. The mechanical behaviour of synthetic, poorly consolidated granular rock under uniaxial compression. Tectonophysics 2003;370(1–4):105–20.
Saidi F, Bernabé Y, Reuschlé T. Uniaxial compression of synthetic, poorly consolidated granular rock with a bimodal grain-size distribution. Rock Mechanics and Rock Engineering 2005;38(2):129–44.
Tippieand DB, Kohlhaas CA. Effect of flow rate on stability of unconsolidated producing sands. In: Proceedings of the 48th Annual Fall Meeting of the Society of Petroleum Engineers of AIME. Las Vegas; 1973. NV, SPE4533.

Dr. Saeed Hashemi is a Lecturer in the field of Geomechanics at CQUniversity in Australia. He received his Ph.D. from the University of Adelaide and his thesis was on "Drilling and maintaining stable boreholes in poorly cemented sands". Saeed holds a M.S. degree in Geotechnical Engineering from the Sharif University (the highest ranked university in Iran), and a BSc degree in Civil Engineering from Iran University of Science and Technology. He is the author of several journal papers in A^+ and A journals (Excellence of Research Australia ranking). Saeed has demonstrated experience in lecturing various geomechanics and rock mechanics courses and in supervising student projects at the University of Adelaide and Sharif University. Besides his academic work experience, Saeed also has more than 7 years of industry work experience where he worked on different construction and oil and gas projects. Saeed received several research grants and awards during his career in Australia, such as Joint Research Engagement Engineering Cadetship Grant, Deep Exploration Technologies CRC, etc. Also, he is a permanent member of Engineers Australia and Organisation for Engineering Order of Buildings in Iran.